J Infrared Milli Terahz Waves (2012) 33:74–81
DOI 10.1007/s10762-011-9847-9

Cancer Diagnosis by Terahertz Molecular Imaging Technique

Seung Jae Oh · Yong-Min Huh · Jin-Suck Suh · Jihye Choi · Seungjoo Haam · Joo-Hiuk Son

Received: 25 January 2011 / Accepted: 10 October 2011 /
Published online: 10 November 2011

Abstract We obtained the diagnostic images of cancerous tumors by employing the THz molecular imaging (TMI) technique which measured the THz response change by surface plasmon resonance induced on the surface of nanoparticles with a irradiation of near-infrared (NIR) beam. To demonstrate the principle of the TMI technique, THz images of tissues with nanoprobes were observed and compared with THz only images. The sensitivity of TMI was further enhanced by adopting a THz differential measurement technique, which was realized by modulating the NIR beams. By employing this differential TMI technique, the diagnostic images of cancerous tumors were obtained *ex vivo* and *in vivo* in the preclinical stage. These images indicated the feasibility of applying the differential TMI technique in the clinical stage.

Keyword Terahertz molecular imaging · Terahertz imaging · Nanoprobe · Nanoparticle

1 Introduction

The terahertz (THz) imaging technique has been employed by various researchers to exploit the unique beneficial properties of THz waves, such as the higher collimination than that of microwaves and the lower Rayleigh scattering than that of infrared and visible beams [1–3].

S. J. Oh · Y.-M. Huh · J.-S. Suh (✉)
Department of Radiology, Medical Convergence Research Institute, Severance Biomedical Science Institute, College of Medicine, Yonsei University, Seoul 120-752, Republic of Korea
e-mail: jss@yuhs.ac

J. Choi · S. Haam
Department of Chemical & Biomolecular Engineering, Yonsei University, Seoul 120-752, Republic of Korea

J.-H. Son (✉)
Laboratory for Terahertz Biophotonics, Department of Physics, University of Seoul, Seoul 130-743, Republic of Korea
e-mail: joohiuk@uos.ac.kr

The energy of THz waves is sufficiently low, so that it does not cause ionization of tissues or cells. Even at THz wave exposure intensities of sub-hundred milliwatt per square centimeter or greater, considerable changes at a cellular and molecular level have not been observed [4]. Hence, it facilitates medical imaging that is safe for human beings [1, 5–7]. It has also been shown that the THz imaging technique is helpful in diagnosing cancerous tumors such as intraepithelial carcinoma, which are difficult to detect early by employing computer tomography (CT), magnetic resonance imaging (MRI), or visible and ultrasonic imaging techniques. The application of THz imaging technique has been extended to a new-generation cancer-diagnosis technique [6, 7]. However, the conventional THz imaging method for cancer diagnosis has monitored the difference of water concentration or the structural change between the cancerous tumor and normal regions, so that it is difficult to identify the miniscule differences at the molecular and cellular levels like the differences between benign and malignant tumors. In order to identify the miniscule differences, it is essential to develop a groundbreaking method for increasing the sensitivity and the target specificity of THz imaging. The sensitivity of THz imaging can be enhanced by employing nanoprobes, as in the case of MRI or optical molecular imaging. The nanoprobe is a nanocomposite that is targeted to specific molecules and directly or indirectly amplifies the responses of image signal with various optical and magnetic characteristics [8–13]. The surface plasmon polaritons (SPP) resonance induced on the surface of the nanoprobe when a near-infrared (NIR) beam is focused on the surface converts most of the NIR energy into heat energy, and as a result, the temperature of the water surrounding the nanoprobe increases. THz waves are much more sensitive to the change of water temperature than infrared and visible beams because most of the characteristic energies of water molecules are in the THz-frequency range [14, 15]. Because of the high thermal sensitivity of THz waves, they can facilitate the measurement of the slight changes in heat resulting from the interaction between the nanoprobes and NIR beam. This principle enables THz molecular imaging (TMI), which can identify the minute differences in the molecular and cellular level using target-specific nanoprobes [8, 9]. In this paper, we demonstrate the concept of the TMI technique and describe the enhancement of the sensitivity of this technique by using a differential detection method. Further, in this study, the diagnostic images of cancerous tumors were obtained *ex vivo* and *in vivo*.

2 Experiments

The TMI system consisted of a 808 nm CW NIR laser for inducing SPP resonance and the reflection-mode THz imaging system for measuring laser-induced temperature change in samples, as shown in Fig. 1. The THz imaging system employed a mode-locked Ti:sapphire laser with center wavelength and pulse width of 800 nm and 80 fs, respectively. The beam produced by this laser was split into pump and probe beams by a beam splitter and the split beams were used to irradiate an InAs semiconductor for generation and a low-temperature-grown (LT)-GaAs antenna for detection. The probe beam was optically delayed using a retroreflector that vibrated at a frequency of 20 Hz and a span of 36 ps. The real-time measurement of THz pulses was carried out by using a digital data acquisition (DAQ) system. The THz pulses emitted from the generator were focused on the sample after passing the waves through two metal parabolic mirrors, and the THz pulses reflected from the sample were guided to the detection antenna using two other parabolic mirrors. The THz spectrum of our system extended from 0.25 to 3 THz,

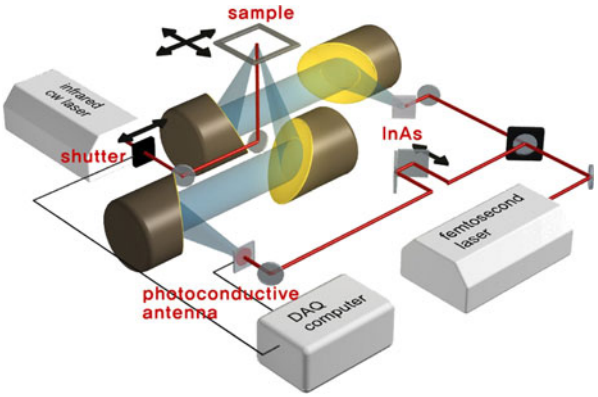

Fig. 1 THz molecular imaging system consisting of a reflection-mode THz imaging setup and a NIR laser.

the peak frequency was 0.5 THz, and the f-number of the optics at the focal point was 1. The diameter of the peak amplitude of THz pulses focused on the sample was 0.8 mm, and the same size NIR laser beam was also illuminated which overlapped with THz beam. The THz imaging system, excluding the sample, was constructed within a dry box so that there could be no effect of humidity on the produced THz signals. The sample was scanned by moving it using a two-dimensional motorized translation stage and the obtained image data were saved and analyzed by a computer.

In order to realize the TMI system, we used gold nanorods (GNRs) as nanoprobes. The GNRs were fabricated by employing a seed-mediated growth technique and the geometry of the GNRs was optimized so that the highest SPP resonance in the NIR region can be realized. The surface of the GNRs was coated with polyethylene glycol (PEG) and modified by Cetuximab, which specifically targets only the cancer cells in which epidermal growth factor receptors (EGFRs) are developed highly. Thus, target-specific Cetuximab-PEGylated gold nanorods (CET-PGNRs) were synthesized and used as the nanoprobes for TMI. For an animal model, A-431 cells were injected subcutaneously in the proximal thigh region of male BALB/c-nude mice that were 5–8 weeks old; these mice were obtained from the Institute of Medical Science (University of Tokyo). All experiments were conducted with the approval of the Association for Assessment and Accreditation of Laboratory Animal Care (AAALAC) International.

3 Results

Figure 2 shows the THz images of liver tissues of mice that were injected with CET-PGNRs and of mice that were not injected with CET-PGNR.As shown in Fig. 2a and b, the difference between the tissues with and without CET-PGNRs cannot be identified by observing the visible and THz images of the tissues obtained when there was no irradiation by NIR laser beam. However, when both the liver tissues were irradiated with NIR beams, the image of the liver tissue with CET-PGNRs was brighter than that without CET-PGNRs, as shown in Fig. 2c. The THz images with and without nanoparticles were subtracted numerically to extract the THz response by the nanoparticles under NIR-beam irradiation. The numerically subtracted image of Fig. 2b and c showed the image of only the liver tissue with CET-PGNRs (Fig. 2d and e). These results revealed that the THz signals were modified as a result of the effect of SPP on the CET-PGNRs under the illumination of NIR

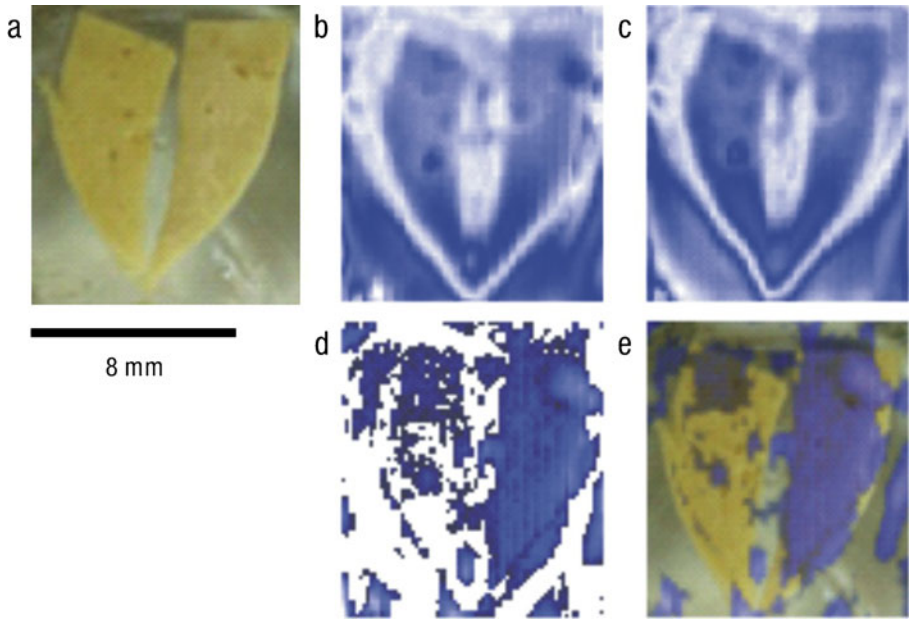

Fig. 2 THz images of liver tissues with and without nanoprobes. **a** Visible image. The left liver was taken from a mouse without injection of nanoparticles and the right one was taken from a mouse with injection of CET-PGNRs. **b** THz image of (**a**). **c** THz image when irradiated with a near-infrared (NIR) beam. **d** Numerically subtracted image of (**b**) and (**c**). **e** Overlapping of (**a**) and (**d**). The intensity of NIR beam is 15 W/cm^2.

beam. This implies that the THz image signals from a sample injected with nanoprobes could be modulated by illuminating with NIR beams having different properties such as different intensities or duty ratios. Thus, numerical subtraction can be realized by directly modulating the NIR beams, and only the part of the tissue with nanoprobes give rise to a signal under differential illumination by NIR beam.

We demonstrated the differential TMI imaging technique by using a solution with nanoprobes. Two kinds of solution samples, one containing CET-PGNRs at a concentration of 100 μM and the other without CET-PGNRs, were prepared as shown in Fig. 3a. An NIR beam with an intensity of 15 W/cm^2 was used to modulate the THz signals. Figure 3b shows the THz images of the sample solutions with and without CET-PGNRs when the samples were not irradiated with NIR beams. When the samples were irradiated with NIR beams, the THz image of the sample solution with CET-PGNRs was brighter than that of the sample solution without CET-PGNRs, as can be seen in Fig. 3c. The numerical subtraction of the images shown in Fig. 3b and c resulted in an image of only the sample solution with CET-PGNRs (Fig. 3d). However, this numerically subtracted image required two different images of the tissue that was irradiated with NIR beams and of the tissue that was not irradiated. This requirement of two images is a critical problem in medical imaging because organs move during measurements as well as the trouble of longer acquisition time. This problem involved in numerical subtraction was overcome by adopting a differential technique in which the THz differential image was constructed by assembling the signals obtained in real time by modulating the NIR beam. Figure 3e and f show the THz differential images obtained by directly modulating the NIR beam. The image was acquired

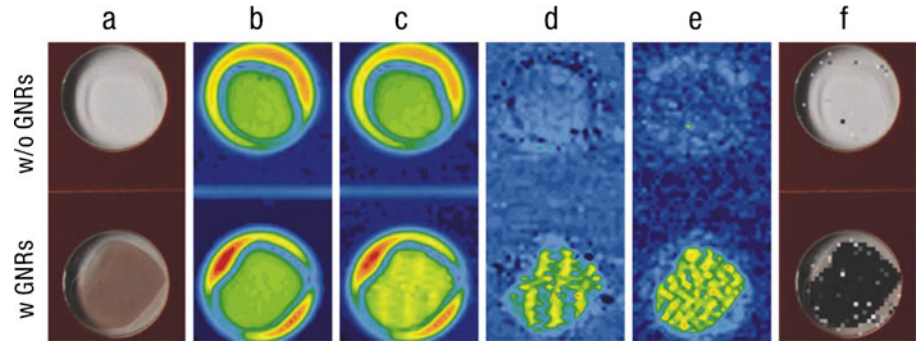

Fig. 3 Comparison between numerically subtracted image and directly modulated differential image. The upper and lower images are of water and of water with nanoparticles, respectively. **a** Visible image. **b** THz image of (**a**). **c** THz image obtained under the illumination of NIR beam. **d** Numerically subtracted image of (**b**) and (**c**). **e** Directly modulated differential THz image. **f** Overlapping of (**a**) and (**e**). The intensity of NIR was 15 W/cm^2. Both the THz and NIR beam diameters were 0.8 mm.

by monitoring the intensity variation of THz signal from temperature change by SPP resonance differentially modulated by NIR beam. If irradiation by the NIR beams was not carried out or if the solution did not contain CET-PGNRs, the THz signal did not change to a null signal. This scheme facilitated the highly sensitive TMI because the intrinsic noise of the THz signal was eliminated as a result of the differentiation of the two signals determined by modulating the NIR beam [8]. The contrast of image achieved when this technique is adopted is higher than that achieved when conventional molecular imaging techniques such as NIR absorption imaging or infrared thermal imaging are adopted [9].

We also obtained the *ex vivo* and *in vivo* diagnostic images of cancerous tumors by the TMI technique. The tissues shown in Fig. 4a and d are A431 epidermoid cancerous tumors extracted from mice that were injected with and those that were not injected with CET-PGNRs; both the tumor tissues were fixed in formalin. An NIR beam with an intensity of 22 W/cm^2 was used to irradiate the sample for 3 s and the exposure conditions of NIR are safe because NIR beams were only minimally absorbed into tissues and cells, although this level exceeds the maximum permissible exposure (MPE) [11, 12]. The sample was moved by 250 μm at a time in order to obtain a two-dimensional image. The time required for obtaining an image was 2 h; however, the acquisition time can be reduced to a few seconds by using a THz camera such as an uncooled, vanadium-oxide microbolometer focal-plane array camera and exploiting the terahertz and NIR source that can illuminate a large area [16]. The difference between the two cancerous tissues could be clearly identified by the existence of CET-PGNRs, as shown in Fig. 4b and e. Figure 4c and f show the three-dimensionally mapped images of Fig. 4b and e. It consistently displayed that the tissue without CET-PGNRs had low intensity signals while the tissue with CET-PGNRs gave strong signals not related with the states of tissues such as the cell structure or humidity.

For animal preclinical stage, several tens of xenograft mouse models with A431 epidermoid carcinoma cells were produced as shown in Fig. 5a and 54 μL of CET-PGNRs at a concentration of 1 mM was injected into the tail vein of the mice. The images of the cancerous tumor were captured 24 h after injection. Figure 5 shows the visible and TMI images of A431 cancerous tumor *in vivo*. The mice with cancerous tumors were affixed to a quartz plate and the region around the tumor was pressed until it was flattened. The mice were alive during and after the experiment. The visible images in Fig. 5b and c show only

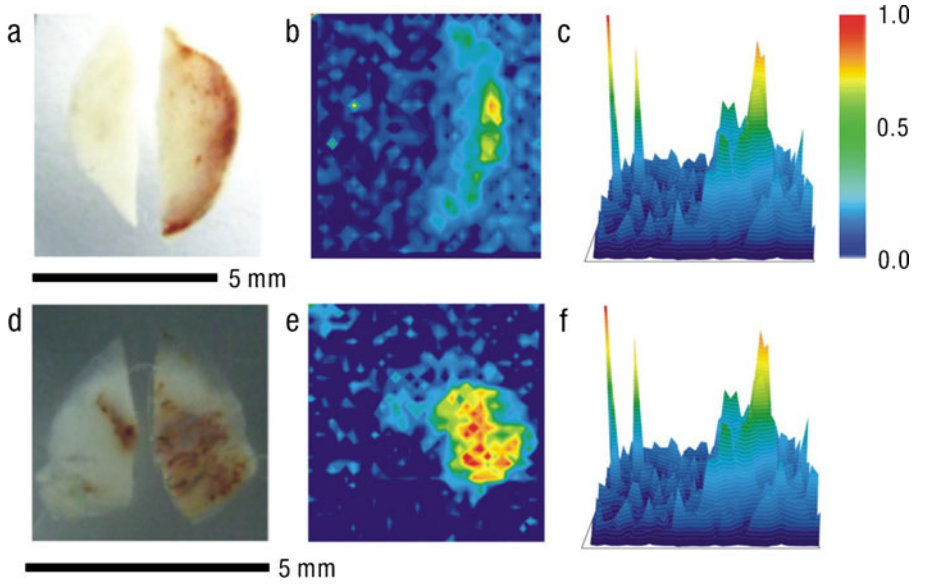

Fig. 4 *Ex vivo* A431 cancer images obtained by the THz differential TMI technique. **a**, **d** Visible images of the A431 cancers. **b**, **e** TMI images of (**a**) and (**d**). **c**, **f** Three-dimensional images of (**b**) and (**e**). The intensity of NIR was 22 W/cm^2.

the superficial form of the tumor that is in the proximal thigh region and do not provide accurate information on the position, size, and type of the tumor. On the other hand, the TMI image in Fig. 5d provides qualitative information on the position and size of the tumor as well as on the type of cancer. The type can be identified because CET-PGNRs were

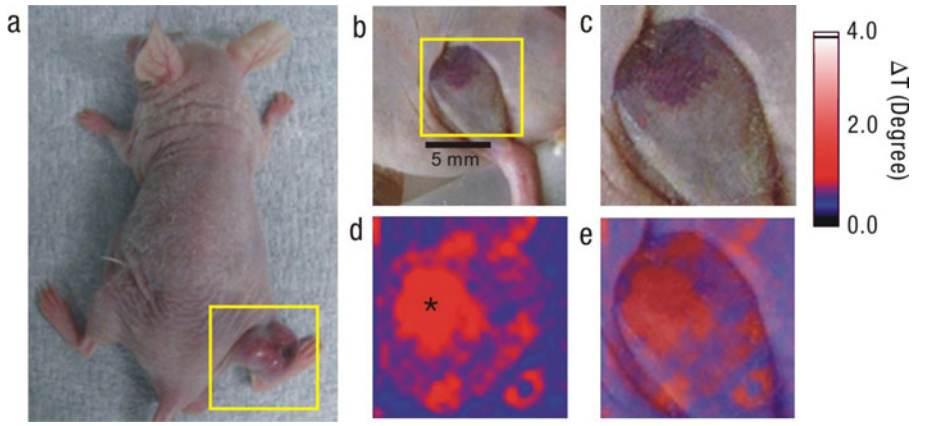

Fig. 5 *In vivo* cancer diagnostic image obtained by the differential TMI technique. **a** Front-view of the mouse with A431 cancerous tumor. **b**, **c** Visible image of the mouse with A431 cancerous tumor. **c** Visible image of the cancerous tumor in the *yellow-outlined box* in (**b**). **d** Directly modulated differential THz image of (**b**). **e** Image obtained by overlapping the images shown in (**c**) and (**d**). The intensity of NIR was 30 W/cm^2, and both the THz and NIR beam diameters were 0.8 mm. The acquisition time of (**d**) is 1 h. An *asterisk* indicated the highest temperature position and the temperature difference at this position was 2.5°.

targeted only to the cell that expressed high levels of EGFR, but could not be absorbed by other cell types [9]. The color scale shown in Fig. 5d and e indicated the degree of temperature change, and it showed the distribution of CET-PGNR in the cancerous tumor. The temperature change in Fig. 5d and e did not exceed 2.5° and the position of the highest temperature position is indicated by an asterisk. The temperature difference at this position was 2.5°. This result implies that the illumination intensity of the laser and the concentration of GNRs are not harmful for tissues *in vivo*. However, when the intensity of NIR and the concentration of nanoparticles are very large, the targeted tissues or cells in the region containing CET-PGNRs are killed because of large heating. This signifies that our technique can also be used as a hyperthermia therapeutic method as well as target-specific imaging.

4 Conclusions

Cancer diagnosis by the terahertz molecular imaging (TMI) technique was demonstrated and *ex vivo* and *in vivo* images of A431 cancerous tumors were obtained. By adopting this technique, we can determine the change in the THz response as a result of surface plasmon resonance on the surface of nanoparticle probes when illuminated with NIR beams. We have also developed a differential measurement technique in which the NIR beam is directly modulated instead of numerical subtraction of two images. This differential measurement technique results in high signal-to-noise ratio because the background noise is eliminated and the high sensitivity arising from the sensitive interaction of THz waves to water. Thus, this technique facilitates target-specific sensing of tumors, and it is also capable of identifying the miniscule differences at a cellular level.

Acknowledgment This study was supported by a grant from the Korean Health Technology R&D Project of the Ministry for Health, Welfare & Family Affairs, Republic of Korea (A101954); a National Research Foundation of Korea (NRF) grants funded by the Ministry of Education Science & Technology, Republic of Korea (20100020647, 20100001979, 20100015989, 20100011934, 20090054519); Business for cooperative R&D between industry, academy, and research institute funded Korea small and medium business administration in 2010 (000428380110).

References

1. J. -H. Son, J. of Appl. Phys. **105**, 102033-1-10 (2009).
2. M. Tonouchi, Nature Photonics **1**, 97-105 (2007).
3. B. Ferguson and X. -C. Zhang, Nature Materials **1**, 26-33 (2002).
4. G. J. Wilmink, B. D. Rivest, C. C. Roth, B. L. Ibey, J. A. Payne, L. X. Cundin, J. E. Grundt, X. Peralta, D. G. Mixon, and W. P. Roach, Laser in Surgery and Medicine **43**, 152-163 (2011).
5. E. Pickwell and V. P. Wallace, J. of Phys. D: Appl. Phys. **39**, R301–R310 (2006).
6. A. J. Fitzgerald, V. P. Wallace, M. Jimenez-Linan, L. Bobrow, R. J. Pye, A. D. Purushotham, and D. D. Arnone, Radiology **239**, 533-540 (2006).
7. R. M. Woodward, V. P. Wallace, R. J. Pye, B. E. Cole, D. D. Arnone, E. H. Linfield, and M. Pepper, J. of Invest. Dermatol. **120**, 72-78 (2003).
8. S. J. Oh, J. Kang, I. Maeng, J. -S. Suh, Y. -M. Huh, S. Haam, and J. -H. Son, Opt. Express **17**, 3469-3475 (2009).
9. S. J. Oh, J. Choi, I. Maeng, J. Y. Park, K. Les, Y. -M. Huh, J. -S. Suh, S. Haam, and J. -H. Son, Opt. Express **19**, 4009-4016 (2011).
10. J. -H. Lee, Y. -M. Huh, Y. -W. Jun, J. -W. Seo, J. -T. Jang, H. -T. Song, S. Kim, E. -J. Cho, H. -G. Yoon, J. -S. Suh, and J. Chen, Nature Medicine **13**, 95-99 (2006).
11. R. Weissleder and V. Ntziachristos, Nature Medicine **9**, 123-128 (2003).

12. J. Lee, J. Yang, H. Ko, S. J. Oh, J. Kang, J. -H. Son, K. Lee, S. -W. Lee, H. -G. Yoon, J. -S. Suh, Y. -M. Huh, and S. Haam, Adv. Func. Mat. **18**, 258-264 (2008).
13. J. Yang, C. -H. Lee, H. -J. Ko, J. -S. Suh, H. -G. Yoon, K. Lee, Y. -M. Huh, and S. Haam, Angew. Chem. Int. Ed. **46**, 8836-8839 (2007).
14. C. Rønne, L. Thrane, P. Åstrand, A. Wallqvist, K. V. Mikkelsen, and S. R. Keiding, J. of Chem. and Phys. **107**, 5319-5331 (1997).
15. J. R. Collins, Phys. Rev. **26**, 771-779 (1925).
16. A. W. M. Lee, B. S. Williams, S. Kumar, Q. Hu, and J. L. Reno, IEEE Photonics Technol. Lett. **18**, 1415-1417 (2006).